THE JOURNAL OF PHYSICAL CHEMISTRY B

Article

Cite This: J. Phys. Chem. B 2018, 122, 4993−5005

pubs.acs.org/JPCB

ONIOM Investigation of the Second-Order Nonlinear Optical Responses of Fluorescent Proteins

Marc de Wergifosse,[†,∥] Edith Botek,[†,⊥] Evelien De Meulenaere,[‡,§,#] Koen Clays,[§] and Benoît Champagne*[,†]

[†]Laboratory of Theoretical Chemistry, Unit of Theoretical and Structural Physical Chemistry, Namur Institute of Structured Matter, University of Namur, Rue de Bruxelles 61, B-5000 Namur, Belgium

[‡]Centre of Microbial and Plant Genetics, KU Leuven, Kasteelpark Arenberg 20, B-3001 Leuven, Belgium

[§]Laboratory for Molecular Electronics and Photonics, Department of Chemistry, KU Leuven, Celestijnenlaan 200D, B-3001 Leuven, Belgium

Supporting Information

ABSTRACT: The first hyperpolarizability (β) of six fluorescent proteins (FPs), namely, enhanced green fluorescent protein, enhanced yellow fluorescent protein, SHardonnay, ZsYellow, DsRed, and mCherry, has been calculated to unravel the structure−property relationships on their second-order nonlinear optical properties, owing to their potential for multidimensional biomedical imaging. The ONIOM scheme has been employed and several of its refinements have been addressed to incorporate efficiently the effects of the microenvironment on the nonlinear optical responses of the FP chromophore that is embedded in a protective β-barrel protein cage. In the ONIOM scheme, the system is decomposed into several layers (here two) treated at different levels of approximation (method1/method2), from the most elaborated method (method1) for its core (called the high layer) to the most approximate one (method2) for the outer surrounding (called the low layer). We observe that a small high layer can already account for the variations of β as a function of the nature of the FP, provided the low layer is treated at an ab initio level to describe properly the effects of key H-bonds. Then, for semiquantitative reproduction of the experimental values obtained from hyper-Rayleigh scattering experiments, it is necessary to incorporate electron correlation as described at the second-order Møller−Plesset perturbation theory (MP2) level as well as implicit solvent effects accounted for using the polarizable continuum model (PCM). This led us to define the MP2/6-31+G(d):HF/6-31+G(d)/IEFPCM scheme as an efficient ONIOM approach and the MP2/6-31+G(d):HF/6-31G(d)/IEFPCM as a better compromise between accuracy and computational needs. Using these methods, we demonstrate that many parameters play a role on the β response of FPs, including the length of the π-conjugated segment, the variation of the bond length alternation, and the presence of π-stacking interactions. Then, noticing the small diversity of the FP chromophores, these results highlight the key role of the β-barrel and surrounding residues on β, not only because they can locally break the noncentrosymmetry vital to a β response but also because it can impose geometrical constraints on the chromophore.

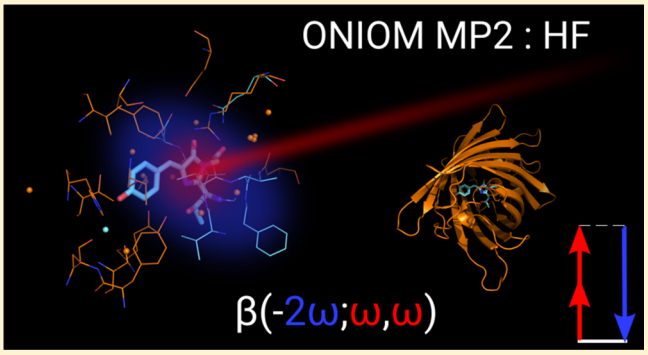

I. INTRODUCTION

Second-harmonic imaging microscopy (SHIM) is a high-resolution biomedical imaging technique that has been developed to reveal structural contrasts originating from variations of noncentrosymmetry in molecular arrangements.[1−10] This technique is highly complementary to two-photon-excitation fluorescence (TPEF) microscopy, which is much better known in the scientific community. In TPEF microscopy, a photon is released upon the relaxation of an excited state obtained by the combined energy of two photons. SHIM is not based on relaxation nor an actual excited state, but photons are collected after a scattering process combining the energy of two photons through a virtual excited state. Both microscopies are nonlinear imaging techniques that can use the same near-infrared incident laser beam, but since SHIM only involves a virtual excited state, damage to biological samples is reduced drastically. SHIM is therefore a powerful noninvasive diagnostic tool for living samples that can probe biological functions and monitor molecular structures in vivo. Information about the molecular organization of chromophores, including structural proteins and dyes and their environment, can be extracted from second-harmonic generation (SHG) imaging

Received: February 9, 2018
Revised: April 20, 2018
Published: April 20, 2018

ACS Publications © 2018 American Chemical Society

DOI: 10.1021/acs.jpcb.8b01430
J. Phys. Chem. B 2018, 122, 4993−5005

data because the SHG signal is polarization-dependent. The SHG polarization anisotropy can simply be used to determine the absolute orientation and the degree of organization of proteins in tissues. On the other hand, TPEF images can be collected in a separate data channel simultaneously to SHG, where polarization anisotropy can also be used, depending on the time decay of the involved excited state. Correlation between SHG and TPEF provides complementary structural information: (i) with TPEF, the location and concentration of chromophores and (ii) with SHIM, noncentrosymmetric molecular arrangements.

The contrast imaging in SHG depends on the molecular orientation of ordered and disordered structures, which can be quantitatively analyzed, as well as on the chromophore intrinsic responses. In biological environments, SHG signals are present in proteins with ordered structures like myosin (mainly α-helices), collagen triple helix,[11−13] and microtubules.[10,14] Dyes can also label biological structures, e.g., voltage-sensitive dyes in membranes to measure membrane potentials. The fine-tuning of molecular properties is required to design dyes for SHG imaging.[2] First, a large first hyperpolarizability (β) at the wavelength of illumination maximizes the SHG signal from the chromophore. Second, SHG dyes with resonance enhancement of β need to have (charge-transfer) bands around the wavelength (one-photon enhancement) and half the wavelength (two-photon enhancement) of the biological tissue transparency window (700−900 nm). Third, an efficient chromophore has high affinity and specificity for the biological targets, e.g., membranes. These considerations need to be tuned to minimize phototoxicity. Probes can also be introduced by genetic modification. The development of fluorescent proteins (FPs) that can be incorporated into organisms by genetic engineering led to the 2008 Nobel Prize in Chemistry awarded to Shimomura, Chalfie, and Tsien.[15−17] Fluorescent proteins of the green fluorescent protein (GFP) family are typically formed by a β-barrel of 235−240 amino acids around a central chromophore.

Several studies have reported the qualitative use of GFP in SHIM,[18,19] and quantitative values for the second-order nonlinear optical (NLO) properties for GFP-like proteins [EGFP, eYFP, ZsYellow (originally called zFP538), DsRed, and mStrawberry] have been determined in the last decade.[20−22] We now know that (i) FP chromophores are able to generate a non-negligible SHG signal that could be used for SHIM and (ii) fluorophores with a more extended π-conjugated linker exhibit larger β values.[22] These experimental findings have been corroborated by quantum chemistry calculations and suggest molecular engineering strategies to produce a full rainbow of FPs for SHIM applications. The SHG response of several FPs is pH-dependent and sensitive to centrosymmetrical elements in or near the chromophore, which was observed as an anomalously low β obtained for the enhanced yellow fluorescent protein (eYFP) that features a centrosymmetrical arrangement between the phenolic Tyr203 residue and the chromophoric Tyr66 moiety. Subsequently, the inversion center of eYFP (Tyr66−Tyr203) was removed by genetic engineering (Tyr66−Phe203), creating a new yellow FP with near-identical linear optical properties but an enhanced SHG response.[23] It was the first time that an FP was altered for this property and an improved fluorescence quantum yield was a welcome side effect. Measurement of β by means of hyper-Rayleigh scattering (HRS) as well as their analysis using quantum chemistry calculations validates this hypothesis. The "fruit" name SHardonnay was proposed for this mutant protein.

In these joint experimental−theoretical investigations,[21−23] although they were able to monitor and interpret the experimental results, at least qualitatively, the ab initio calculations assume two major approximations: (i) the calculations were focusing on the properties of the chromophores with or without a few surrounding amino acid residues so that the largest part of the β-barrel was modeled using the polarizable continuum model and (ii) they were carried out at the Hartree−Fock (HF) level, which brings the question about the impact of electron correlation. However, although nowadays proteins are still too large to allow determining their SHG responses ab initio, approximate schemes are available to account for the effects of the surrounding. Among them, the our own N-layered integrated molecular orbital and molecular mechanics (ONIOM) method[24−27] consists in partitioning the system in several layers treated at different levels of theory. In the two-layer ONIOM approximation, the system is partitioned in high and low layers. The high/low ONIOM layer is the part of the system, which is investigated by a high/low level of theory. To get the extrapolated ONIOM energy, E_{ONIOM}, three calculations are needed. First, the energy of the entire (real) system is calculated with the low-level method, $E_{\mathrm{real,low}}$. The second and third calculations provide the energy of the model system at low and high levels of theory, $E_{\mathrm{model,low}}$ and $E_{\mathrm{model,high}}$, respectively. The extrapolated ONIOM energy reads

$$E_{\mathrm{ONIOM}} = E_{\mathrm{model,high}} + E_{\mathrm{real,low}} - E_{\mathrm{model,low}}$$

The extrapolated ONIOM first hyperpolarizability tensor $\vec{\vec{\beta}}_{\mathrm{ONIOM}}$ is obtained in the same way since the ONIOM scheme allows for a consistent treatment of the molecular properties, originating from responses with respect to static and dynamic electric fields[24−27]

$$\begin{aligned}\vec{\vec{\beta}}_{\mathrm{ONIOM}} &= \vec{\vec{\beta}}_{\mathrm{model,high}} + \vec{\vec{\beta}}_{\mathrm{real,low}} - \vec{\vec{\beta}}_{\mathrm{model,low}} \\ &= \vec{\vec{\beta}}_{\mathrm{model,high}} + \vec{\vec{\beta}}_{\mathrm{environment}}\end{aligned}$$

where the last equality defines the environment contribution to the β tensor. The ONIOM method was already employed to treat fluorescent proteins for characterizing mechanistic pathways, magnetic exchange coupling constants, as well as absorption, emission, vibrational, and Raman spectra.[28−34] For example, in ref 28, competitive mechanistic pathways for green-to-red photoconversion in Kaede FP were investigated with explicit consideration of the protein environment using ONIOM(B3LYP:AMBER) calculations, concluding that the stepwise "E1" and "E1cb" mechanisms occur and compete with each other in the electronic ground state. Then, in ref 29, the nature of the ON and OFF states of reversible photoswitching Dronpa were studied by ONIOM(QM:MM) calculations. Alternative QM:MM schemes have also been employed to study two-photon absorption in FPs in relationship with linear optical properties, UV/vis absorption and emission spectra,[35−37] but the applications to SHG are scarce.

In this paper, we address the performance of different computational methods to predict and analyze the first hyperpolarizability of FPs. For this purpose, six FPs were selected: eGFP, eYFP, SHardonnay, ZsYellow, DsRed, and mCherry. In particular, we apply the ONIOM scheme at

DOI: 10.1021/acs.jpcb.8b01430
J. Phys. Chem. B 2018, 122, 4993−5005

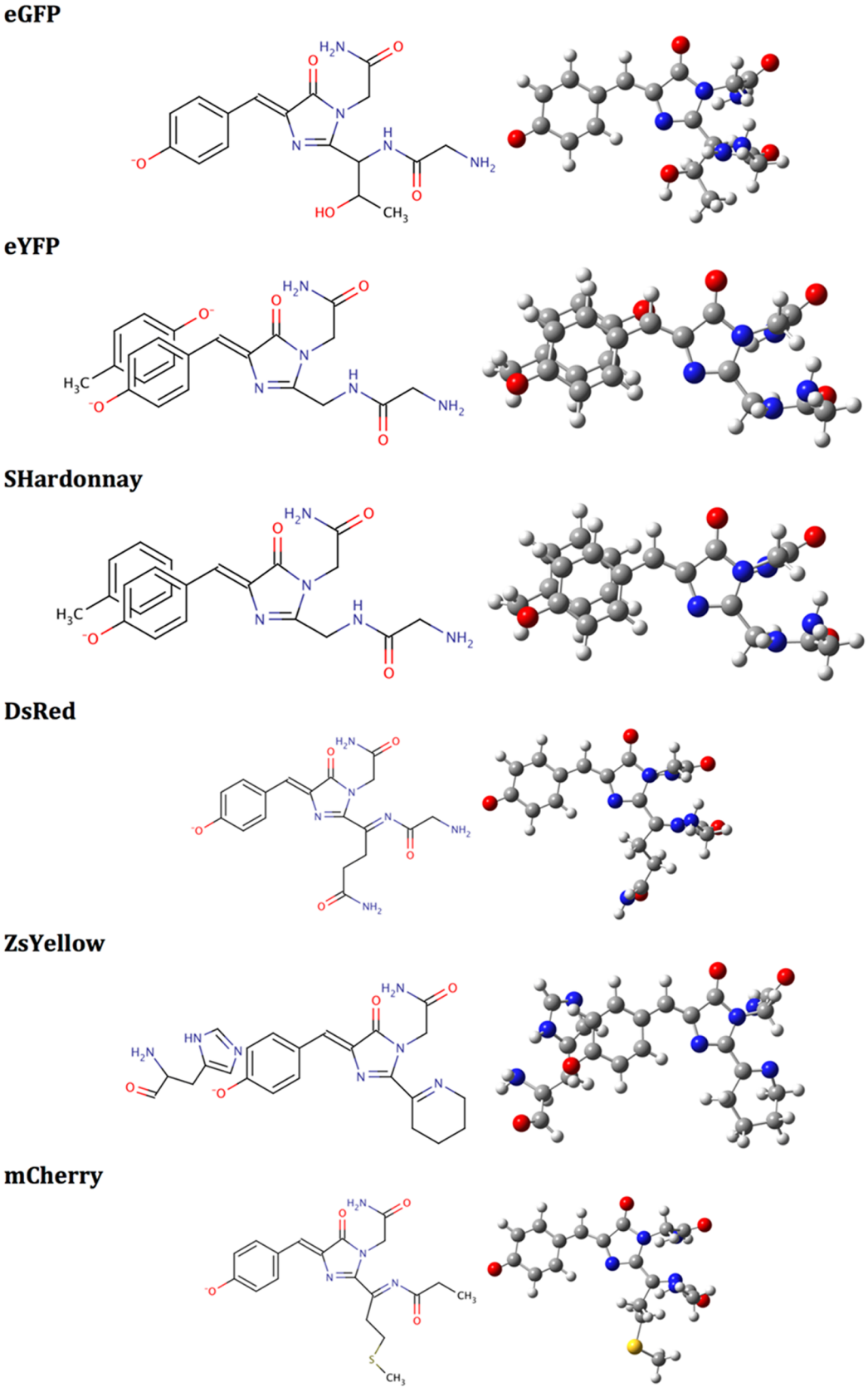

Figure 1. Structures of the eGFP, eYFP, SHardonnay, DsRed, ZsYellow, and mCherry deprotonated chromophores with the directly interacting π-stacked residues, when present. The structures on the right-hand side were obtained by optimizing the H-atom positions at the B3LYP/6-31+G(d) level.

DOI: 10.1021/acs.jpcb.8b01430
J. Phys. Chem. B 2018, 122, 4993−5005

Table 1. Successive Compositions of the ONIOM High Layers for the Different FPs[a]

	first high layer (FHL)	second high layer (SHL)	third high layer (THL)
eGFP	chromophore	FHL + GLN 94	SHL + H_2O
eYFP	chromophore + TYR 203	FHL + ARG 96	SHL + H_2O
SHardonnay	chromophore + PHE 203	FHL + ARG 96	SHL + HIS 148 + H_2O
ZsYellow	chromophore + HIS 202	FHL + ARG 95	SHL + SER 148 + H_2O
DsRed	chromophore	FHL + ARG 95	SHL + SER 146 + $2H_2O$
mCherry	chromophore	FHL + ARG 95	SHL + SER 146 + $2H_2O$

[a]Note here that "chromophore" refers to the "naked" chromophore with those covalently bonded amino acids that present interactions with the chromophore since the residues chain is folded around it.

successive levels of refinement compared to reference calculations carried out on the entire systems. In the case of ONIOM β calculations, all layers must preferentially be described at a quantum chemical level, which allows for several combinations of methods and layers. Still, on the one hand, the low level of treatment uses here either the HF method with a more or less reduced basis set with respect to the one used for the high level or the semiempirical PM6 method.[38] On the other hand, for the high level adopted to describe the core system, the HF method and preferentially correlated ab initio methods are systematically used. Indeed, the effects of electron correlation on β are far from being negligible for push−pull π-conjugated systems.[39−43] Nowadays, for small polyatomic molecules, the most efficient and accessible description is given by coupled cluster singles and doubles calculations with perturbative estimate of triples [CCSD(T)], but this method cannot be routinely applied to large systems. Then, because of cancelations between higher-order contributions, the MP2 method often turns out to be the method of choice to predict β of push−pull π-conjugated systems since it closely reproduces the values obtained with the reference CCSD(T) scheme.[42] Among density functional theory (DFT) exchange−correlation (XC) functionals, LC-BLYP is reliable when characterizing the changes of β upon enlarging the π-conjugated linker in a polyene segment.[42] Nevertheless, its reliability is very similar to what can be achieved with the HF method. Moreover, for the model system, the ab initio calculations should use more extended basis sets, appropriate to describe the nonlinear response of the molecule to external electric fields, such as the 6-31+G(d) basis set.

This article is organized as follows. In Section II, we summarize the theoretical and computational approaches. Section III presents and discusses the results obtained using successive approximate schemes. Then, before concluding in Section V, Section IV presents comparisons with available experimental data, highlighting the improvements that could be achieved by going to higher and higher levels of approximation.

II. THEORETICAL AND COMPUTATIONAL ASPECTS

The geometries of the chromophores surrounded by their first shell of residues (including water molecules and amino acids from the protein β barrel) were taken from X-ray diffraction data.[44−48] The resolutions of the X-ray data are 2.25, 2.50, 2.00, 1.95, 1.36, and 2.70 Å for eGFP, eYFP, DsRed, SHardonnay, mCherry, and ZsYellow, respectively. The missing H atoms were added by considering structural aspects, and their positions were optimized at the PM6 level of calculation with the MOPAC package.[49] The rest of the geometry was kept frozen to maintain the chromophore in its natural conformation. These systems contain 405, 476, 483, 465, 549, and 561 atoms for eGFP, eYFP, SHardonnay, DsRed, ZsYellow, and mCherry, respectively. On the other hand, we also considered smaller model systems containing only the chromophore with the directly interacting residues (i.e., TYR 203 for eYFP, PHE 203 for SHardonnay, and HIS 202 for ZsYellow; Figure 1). In that case, the H atom positions were optimized at the DFT level with the B3LYP XC functional and the 6-31+G(d) basis set.

The ONIOM scheme was used to evaluate β of the systems composed of the chromophore surrounded by its first shell of residues. To probe the minimal requirement for the size of the high layer, the calculations used successive definitions of the ONIOM layers, where the number of residues is increased in the high layer (Table 1). The smallest high layer is defined by the naked chromophore and covalently linked residues as well as key residues like Tyr203 for eYFP. The next high layers include H-bond interactions with surrounding residues or water molecules (Figure 2).

Static and dynamic β values of the structures presented in Figure 1 were calculated (i) at the coupled-perturbed HF (CPHF) level to evaluate the static responses; (ii) using the time-dependent HF (TDHF) scheme to describe frequency dispersion (at wavelengths of 1064 and 1900 nm); and (iii) with DFT (and time-dependent density functional theory, TDDFT) as well as with MP2 to account for electron correlation effects. Consistently with ref 42, the 6-31+G(d) basis set was used. Additional 6-31G(d) calculations were also performed at the MP2 level. At that level, only the static values were evaluated by employing the finite-field procedure.[50−52] Then, the multiplicative scheme was used to estimate the dynamic MP2 β values. DFT/TDDFT calculations adopted the LC-BLYP XC functional (with a range-separating parameter (μ) of 0.47), as well as the widely used B3LYP functional for comparison.

In the ONIOM calculations, the HF/6-31+G(d) method was used to treat the high layer and additional calculations were performed at the LC-BLYP/6-31+G(d) and MP2/6-31+G(d) levels to account for electron correlation. We note that provided the same basis set is used for both layers, the MP2:HF ONIOM expression simplifies to

$$\vec{\vec{\beta}}_{\mathrm{ONIOM}} = \vec{\vec{\beta}}_{\mathrm{real,HF}} + \vec{\vec{\beta}}_{\mathrm{model,E2}}$$

where E2 is the second-order perturbation theory correction. For the low layer, the PM6 method was first chosen and comparisons were performed with HF/3-21G and HF/6-31G(d) levels of theory. We note that unpublished results on the push−pull π-conjugated systems of ref 42 show that for doubly bonded systems, PM6 systematically underestimates the reference CCSD(T) β values by about 32−38%, which corresponds to a smaller underestimation than the HF method. Thus, PM6 appears to account implicitly for some electron

DOI: 10.1021/acs.jpcb.8b01430
J. Phys. Chem. B 2018, 122, 4993−5005

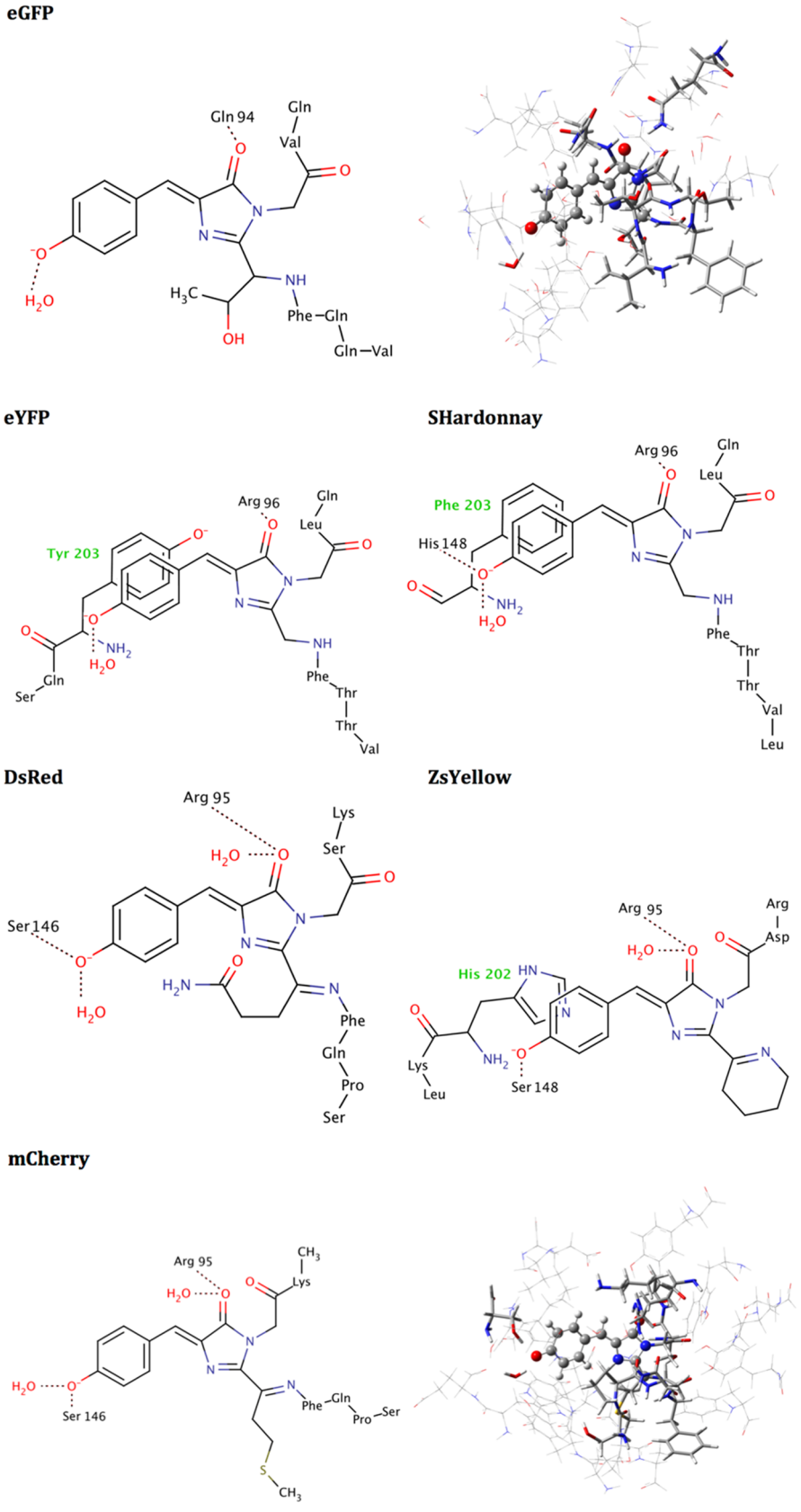

Figure 2. Structures of the largest ONIOM high layers (third high layer, THL) for eGFP, eYFP, SHardonnay, DsRed, ZsYellow, and mCherry. The full structures, i.e., with the whole first shell of residues, of eGFP and mCherry are also represented (chromophore in [balls and sticks], third high layer in [balls and sticks + thick sticks], and low layer in [thin sticks]).

DOI: 10.1021/acs.jpcb.8b01430
J. Phys. Chem. B 2018, 122, 4993−5005

Table 2. Static and Dynamic First Hyperpolarizabilities (au) of the Deprotonated Chromophores with Part of Their Protein Environment Calculated at Different Levels of Approximation within the ONIOM Formalism[a]

β_{HRS} IEFPCM (water)	∞	1900 nm	1064 nm	∞	1900 nm	1064 nm	∞	1900 nm	1064 nm
		eGFP			*eYFP*			*SHardonnay*	
high model		FHL			FHL			FHL	
HF/6-31+G(d):PM6	6108	3492	5731	4953	3009	5068	2897	3371	5997
HF/6-31+G(d):HF/3-21G	5709	3187	5613	5261	3035	5334	4565	3001	4880
HF/6-31+G(d):HF/6-31G(d)	5536	3137	5614	5240	3075	5444	4692	3042	5022
high model		SHL			SHL			SHL	
HF/6-31+G(d):PM6	6515	3727	6054	4806	2965	5016	2787	3147	5537
high model		THL			THL			THL	
HF/6-31+G(d):PM6	6182	3607	5938	4863	2903	4843	4274	3072	4950
full calculation									
HF/6-31G(d)	4991	2985	5149	4806	2936	5004	4397	2976	4779
HF/6-31+G(d)	5060	2973	5356	5016	3295	5430	4518	3012	4925
		ZsYellow			*DsRed*			*mCherry*	
high model		FHL			FHL			FHL	
HF/6-31+G(d):PM6	6709	4092	10 342	8650	5567	15 084	9836	6917	28 566
HF/6-31+G(d):HF/3-21G	6171	3639	9006	9330	5554	13 495	12 584	6929	23 695
HF/6-31+G(d):HF/6-31G(d)	6153	3730	9160	9041	5442	12 951	12 610	7121	22 892
high model		SHL			SHL			SHL	
HF/6-31+G(d):PM6	6551	4026	10 435	8457	5489	15 044	9698	6988	30 282
high model		THL			THL			THL	
HF/6-31+G(d):PM6	6750	4207	10 544	8478	5433	12 864	11 777	7235	22 211
full calculation									
HF/6-31G(d)	5837	3667	8315	8202	5138	11 366	11 368	7212	19 618
HF/6-31+G(d)	6100	4053	8921	8675	5385	12 453	12 405	7329	29 895

[a]Solvent effects were accounted for using the IEFPCM scheme.

correlation effects. Since β values have been rarely calculated within the ONIOM procedure,[11,23] TDHF and CPHF calculations were also carried out for the entire system and compared to the successive ONIOM results.

The polarizable continuum model within the integral equation formalism (IEFPCM) was used to account for solvent effects.[53,54] In the ONIOM method, for each subcalculation, the cavity of the real system was used,[55] which corresponds to the so-called ONIOM/PCM-X scheme. This approach was selected since it can easily include solvent effects in ONIOM finite-field calculations. Solvents with decreasing static and dynamic dielectric constants were considered, namely, water (ε_0 = 78.355, ε_∞ = 1.7778), ethanol (ε_0 = 24.852, ε_∞ = 1.8525), 1-butanol (ε_0 = 17.332, ε_∞ = 1.9580), 1-heptanol (ε_0 = 11.321, ε_∞ =2.0303), and 1-decanol (ε_0 = 7.530, ε_∞ =2.0655). Of course, the FPs are not necessarily soluble in all of these solvents, which is not an issue here since we aim at studying the effects of the dielectric constant. This traditional PCM approach accounts for the reaction field effects between the chromophore and the solvent, whereas the presence of the surrounding residues, which screen the external electric field, accounts partly for the effects of the cavity field.

The targeted first hyperpolarizability quantities correspond to those that are extracted from hyper-Rayleigh scattering (HRS) measurements, β_{HRS}, for a nonpolarized incident light and detection of the SHG intensity of the vertically polarized signal scattered at 90° with respect to the propagation direction. Depolarization ratios (DRs) were also calculated to assess the dipolar versus octupolar character of the chromophore. All reported β_{HRS} values are given in au within the T convention. All calculations were carried out using the Gaussian 09 package.[56]

III. RESULTS AND DISCUSSION

III.A. Comparison between Full CPHF/TDHF and ONIOM Results. Tables 2 and S1 present the ONIOM static and dynamic β values calculated with and without including solvent effects. Three ONIOM treatments are considered, i.e., HF/6-31+G(d):PM6, HF/6-31+G(d):HF/3-21G, and HF/6-31+G(d):HF/6-31G(d), in combination with each of the three high models described in Table 1. These results are compared to those obtained on the full systems (without the ONIOM partitioning) to assess the quality of the ONIOM layering. First, we make the comparison for the static β by considering ONIOM with the FHL and IEFPCM to describe solvent (water) effects. For eGFP, the agreement with the reference improves with the level of treatment of the low layer from PM6 (21% of overestimation) to HF/3-21G (13%) and HF/6-31G(d) (9%). Similar behaviors are observed for ZsYellow and mCherry, leading to very small differences (1−2%) at the HF/6-31+G(d):HF/6-31G(d) level with respect to the full calculation. For eYFP and DsRed, the difference with the

DOI: 10.1021/acs.jpcb.8b01430
J. Phys. Chem. B 2018, 122, 4993−5005

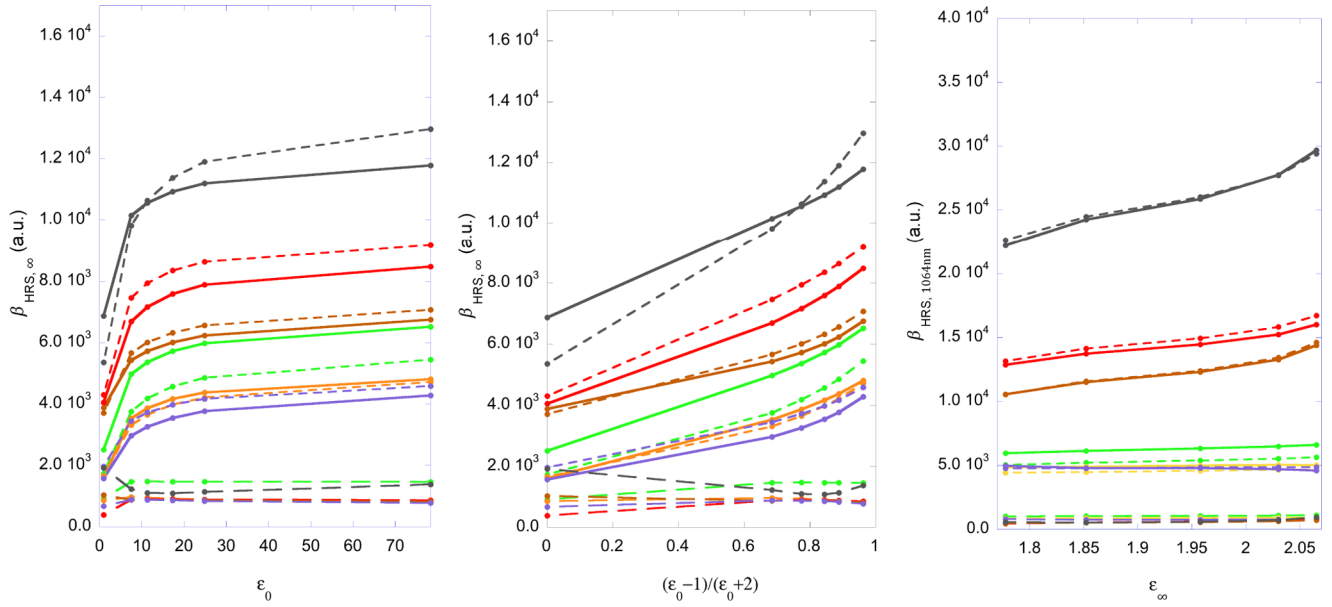

Figure 3. Static (left and middle) and dynamic (λ = 1064 nm, right) HRS first hyperpolarizability [β_{ONIOM} (solid line), $\beta_{model,high}$ (short-dashed line), and $\beta_{environment}$ (long-dashed line)] in eGFP (green), eYFP (orange), SHardonnay (purple), DsRed (red), ZsYellow (brown), and mCherry (dark gray) as a function of the solvent static/dynamic dielectric constant [ε_0 (left) and ε_∞ (right)] or as a function of $(\varepsilon_0 - 1)/(\varepsilon_0 + 2)$ (middle). The calculations were carried out at the ONIOM HF/6-31+G(d):PM6 level with the THL.

reference increases, but the agreement remains good (4−5% overestimation) when the low layer is described at the HF/6-31G(d) level. On the other hand, in the case of SHardonnay, the PM6 method fails to describe the environment as evidenced by a 36% underestimation of the static β. Then, using the HF/6-31+G(d):HF/3-21G and HF/6-31+G(d):HF/6-31G(d) levels of treatment restores the agreement with overestimations of 1 and 4%, respectively. From these comparisons, one can conclude that the FHL is sufficient, provided the remaining part of the system is treated ab initio, preferentially with the 6-31G(d) basis set.

Additional calculations were then performed by enlarging the high layer, from FHL to SHL and THL, while keeping the PM6 method for describing the outer region. With the exception of SHardonnay and mCherry, the impact of enlarging the high layer is small, in particular in view of the difference with respect to the reference results. For instance, for eGFP, starting from the smallest high-layer model, by adding GLN 94 and then a water molecule, the β_{ONIOM} overestimation goes from 21 to 29%, and then to 22%. In the case of SHardonnay, there is a strong impact when including in the high layer the H-bonds with ARG 96, HIS 148, and a water molecule (THL), and it results in an underestimation as small as 6%, in comparison to the 36% underestimation for the FHL. Thus, the PM6 method fails to describe the response dependence of the strong H-bond between the HIS 148 and the chromophore ($d_{O\cdots H}$ = 1.794 Å). In the case of mCherry, the 20% difference observed for the FHL with respect to the reference decreases substantially to 5% in the case of the THL, where H-bonds are included in the HF treatment. As complementary intermediate conclusion, the HF:PM6 ONIOM method gives a good compromise between accuracy and calculation resources, provided the key H-bonds are included in the high layer. Still HF:HF ONIOM schemes are preferable when aiming at reducing the size of the high layer.

The analysis performed on the static first hyperpolarizability remains valid for the dynamic quantities. In fact, at λ = 1900 nm, using the HF/6-31+G(d):PM6 scheme in combination with the FHL always gives a 10−15% agreement or even better with the reference results. Then, with the exception of ZsYellow, this agreement is improved when using the HF/6-31+G(d):HF/6-31G(d) scheme. At λ = 1064 nm, this behavior is observed again, although near-resonance effects might appear like in the case of the HF/6-31+G(d):HF/3-21G and HF/6-31+G(d):HF/6-31G(d) calculations on mCherry. These correspond to large enhancement of β from 1900 to 1064 nm.

III.B. Solvent or Dielectric Effects. The surrounding effects beyond the residues forming a shell around the chromophore, i.e., beyond what is included in the ONIOM calculations, are described using the IEFPCM approach. An obvious choice for the solvent is water because the proteins contain water molecules. However, the surrounding is also made of amino acid residues that can be approximated by a dielectrics with a lower dielectric constant than water. So, water as solvent is expected to provide an upper limit to the effects of the surrounding beyond the first amino acids shell on β. This led us to assess the range of variations of β as a function of the solvent. Figures 3 and S1 present for the successive FHL, SHL, and THL (Table 1) the HF/6-31+G(d):PM6 static first hyperpolarizabilities as a function of the dielectric constant of the solvent used in the IEFPCM treatment compared to the in vacuo values. The contributions of $\beta_{model,high}$ and $\beta_{environment}$ are also reported. The largest variation of β occurs for small ε_0 values, typically between the results obtained in vacuo and those with 1-decanol (ε_0 = 7.530). Then, β evolves slowly and smoothly toward the value in water. Then, analyzing the evolution of β as a function of the Clausius−Mossotti $(\varepsilon_0 - 1)/(\varepsilon_0 + 2)$ function gives an almost linear relationship, with a nonlinear enhancement for larger ε_0 values. Provided the THL is used, the β contribution of the environment is always small with respect to the response of the high layer or of the whole system (Figure 3). Similar observations are made for the FHL and SHL (Figure S1) with the exception of SHardonnay and mCherry, which require including more residues in the high

DOI: 10.1021/acs.jpcb.8b01430
J. Phys. Chem. B 2018, 122, 4993−5005

Table 3. Static and Dynamic β_{HRS} (au) of the Deprotonated Chromophores Sketched in Figure 1 Calculated at the IEFPCM (Water)/MP2/6-31+G(d) Level[a]

	HF		MP2	
	$\lambda = \infty$	$\lambda = \infty$	λ = 1900 nm	λ = 1064 nm
eGFP	7171 (0.463)	15 482	7075	12 414
eYFP + TYR 203	5752 (0.438)	13 134	6242	11 146
SHardonnay	6670 (0.373)	17 897	9943	17 321
ZsYellow + HIS 202	8059 (0.461)	17 481	9656	24 845
DsRed	9026 (0.458)	19 710	10 745	22 482
mCherry	15 069 (0.455)	33 130	19 868	62 918

[a]The dynamic values were calculated using the multiplicative scheme and the TDHF/CPHF data of Table S3. The second column reports the IEFPCM(water)/CPHF/6-31+G(d) values as well as, in parentheses, their ratios with respect to the reference MP2 static values, β(HF)/β(MP2).

Table 4. IEFPCM (Water)/DFT Static and Dynamic β_{HRS} (au) of the Deprotonated Chromophores Sketched in Figure 1 Calculated with the 6-31+G(d) Basis Set Using the B3LYP and LC-BLYP XC Functionals[a]

	B3LYP			LC-BLYP		
	∞	1900 nm	1064 nm	∞	1900 nm	1064 nm
eGFP	4688 (0.303)	2274	6397	9474 (0.612)	4570	11 200
eYFP + TYR 203	4462 (0.340)	2658	5160	8638 (0.658)	4160	10 206
SHardonnay	9262 (0.518)	4715	18 043	11 887 (0.664)	6487	14 847
zFP538 + HIS 202	10 031 (0.574)	7374	816 748	10 727 (0.614)	6529	27 751
DsRed	13 811 (0.701)	9813	194 599	11 961 (0.607)	7047	23 037
mCherry	13 260 (0.400)	8718	72 699	18 709 (0.565)	11 683	90 351

[a]The β(DFT)/β(MP2) ratios are reported in parentheses for the static quantities.

layer. This is consistent with the results of Section III.A. Considering the THL in the calculations, for both β_{ONIOM} and $\beta_{model,high}$, the static HF β_{HRS} values increase in the following order (SHhardon. = SHardonnay, ZsY = ZsYellow)

SHardon. < eYFP < eGFP < ZsY < DsRed < mCherry

Since all H-bonds less than 2 Å are included in the THL, the $\beta_{environment}$ contributions to SHardonnay, DsRed, and mCherry responses are reduced and are of similar amplitudes to those of the other FPs.

Then, the analysis has been extended to the dynamic responses calculated for a wavelength of 1064 nm (Figures 3 and S2). Considering the narrow range of optical dielectric constants (ε_∞), the first hyperpolarizability is hardly influenced by the nature of the solvent. This demonstrates that it is obvious to choose water as solvent for describing the dynamic first hyperpolarizabilities since it is the solvent used in the experiment and that other solvents have mostly the same effect, besides under near-resonance conditions. In the case of the dynamic responses as calculated using the THL and including solvent (water) effects, the β_{ONIOM} values follow this ordering

eYFP ≈ SHardon. < eGFP < ZsY < DsRed < mCherry

This demonstrates that the correct (experimental) ordering (see Table 6 in Section IV) of the β_{HRS} responses of eYFP and SHardonnay requires accounting for frequency dispersion effects. On the other hand, the relative β_{HRS} values of the other FPs are not modified.

III.C. Electron Correlation Effects. Table 3 presents the static β_{HRS} of the deprotonated chromophore calculated at the MP2/6-31+G(d) level with water as solvent in comparison to the corresponding CPHF values, demonstrating that the inclusion of electron correlation effects leads to an increase of β_{HRS} by a factor larger than 2. Table S2 provides complementary data, showing that (i) similar β(MP2)/β(HF) ratios are obtained when replacing the 6-31+G(d) basis set by 6-31G(d), but that (ii) in vacuo, the β(MP2)/β(HF) ratios vary strongly among the FPs. Table 3 also reports the dynamic MP2 responses as obtained by scaling the static MP2 values by the TDHF/CPHF ratios. At this level (MP2, $\lambda = \infty$ or 1900 nm), the β_{HRS} ordering becomes

eYFP < eGFP < ZsY ≈ SHardon. < DsRed < mCherry

As discussed below, the relative β_{HRS} values of eYFP, eGFP, and SHardonnay are now consistent with experiment. Electron correlation effects were also described at the IEFPCM(water)/DFT/6-31+G(d) level using the B3LYP and LC-BLYP XC functionals. Table 4 shows that the β(B3LYP)/β(MP2) ratios are also smaller than 1, like at the HF level, but that they vary much more as a function of the nature of the FP, from 0.30 for eGFP to 0.70 for DsRed. An a posteriori correction of the B3LYP β_{HRS} values is therefore less feasible than from the HF values, substantiating previous reports on the drawback of B3LYP XC functionals to screen the first hyperpolarizability of chromophores of different π-conjugated lengths and compositions.[39,42] Indeed, using global hybrids with less than 100% of HF exchange, the exchange contribution does not exhibit the complete and correct $-1/r$ long-range behavior. Moreover, the β_{HRS} ordering is very different from the ordering at the MP2 level with puzzling inversions between eGFP and eYFP as well as between DsRed and mCherry. On the other hand, the LC-BLYP XC functional systematically underestimates the MP2 values by 33−40%, but it allows more accurate predictions of structure−β_{HRS} relationships and restores the relative ordering of the β_{HRS} of the eGFP/eYFP and DsRed/mCherry pairs.

The MP2/6-31+G(d) correlated treatment was then employed within the ONIOM frame in combination with the PM6, HF/6-31G(d), and HF/6-31+G(d) methods to describe the low layer. As evidenced in Table 5, like for the isolated chromophore, the IEFPCM β_{HRS} values increase by about a factor of 2 ± 0.3 for all FPs, except for SHardonnay, where β_{HRS} gets 3 times larger. When the calculations are performed

DOI: 10.1021/acs.jpcb.8b01430
J. Phys. Chem. B 2018, 122, 4993−5005

Table 5. Static and Dynamic β_{HRS} (au) of the Deprotonated Chromophores in Its Protein Environment as Calculated at the ONIOM MP2:HF 6-31+G(d) Level[a]

	in vacuo			in water (IEFPCM)		
	∞	1900 nm	1064 nm	∞	1900 nm	1064 nm
eGFP	1558 (0.938)	1895	3341	8448 (1.670)	4965	8945
eYFP	2784 (1.716)	3334	5551	9232 (1.840)	6063	9991
SHardonnay	4721 (2.684)	5529	8562	14 073 (3.115)	9382	15 340
ZsYellow	6885 (2.087)	9325	25 847	14 165 (2.322)	9411	20 715
DsRed	7334 (1.770)	9755	24 826	17 899 (2.063)	11 109	2569
mCherry	7251 (1.255)	10 587	47 777	26 383 (2.127)	15 589	63 587

[a]The ONIOM high layer is defined as the chromophore and some crucial residues [TYR 203 (eYFP), PHE 203 (SHardonnay), and HIS 202 (ZsYellow)]. The ratios between the MP2:HF ONIOM calculations and the full HF results are given in parentheses in the second and fifth columns for the static quantities.

Table 6. β_{HRS} (in 100 au) for eGFP, eYFP, SHardonnay, ZsYellow, DsRed, and mCherry, as Determined from Measurements Performed at 800 nm (refs 8−10) and the Corresponding Values Extrapolated to Static Limit[a]

	eGFP	eYFP	SHardonnay	ZsYellow	DsRed	mCherry
Exp., 800 nm	248 ± 39	86 ± 9	185 ± 12	208 ± 12	188 ± 19	310 ± 38
Exp., ∞ nm	44 ± 7 (0.27)	30 ± 5 (0.19)	63 ± 5 (0.39)	76 ± 5 (0.47)	76 ± 7 (0.47)	162 ± 21
HF:PM6 (THL, IEFPCM)	41 (0.48)	39 (0.46)	49 (0.58)	53 (0.62)	75 (0.88)	85
HF (full, IEFPCM)	30 (0.41)	33 (0.45)	30 (0.41)	41 (0.56)	54 (0.74)	73
HF (full, vacuo)	20 (0.24)	19 (0.23)	21 (0.25)	45 (0.54)	55 (0.65)	84
HF (chromo, IEFPCM)	33 (0.37)	27 (0.30)	37 (0.41)	45 (0.50)	49 (0.54)	90
MP2 (chromo, IEFPCM)	71 (0.36)	62 (0.31)	99 (0.50)	97 (0.49)	107 (0.54)	199
MP2:PM6 (IEFPCM)	58 (0.36)	54 (0.34)	140 (0.86)	96 (0.60)	110 (0.68)	161
MP2:HF (IEFPCM)	50 (0.32)	61 (0.39)	94 (0.60)	94 (0.60)	111 (0.71)	156
MP2:HF (vacuo)	19 (0.18)	33 (0.35)	55 (0.53)	93 (0.54)	98 (0.68)	106

[a]These values are compared to those calculated at different levels of approximation. For the calculations, only 6-31+G(d) basis set and λ = 1900 nm results are reported. The ratios with respect to mCherry are given in parentheses.

without considering the solvent, the HF-to-MP2 enhancements are also very similar to those observed for the isolated chromophore, showing that the electron correlation effects are not much impacted by the surrounding low layer. The corresponding β_{HRS} ordering reads

$$\text{eGFP} < \text{eYFP} < \text{ZsY} \approx \text{SHardon.} < \text{DsRed} < \text{mCherry}$$

Table S4 provides additional data showing that the β_{HRS} variations are small and generally smaller than 5% when using the HF/6-31G(d) method instead of the HF/6-31+G(d) one for the low layer, which turns out to be a good compromise between accuracy and computational requirements because the replacement of HF/6-31+G(d) by HF/6-31G(d) for the low layer results in a speed-up by a factor of 15. On the other hand, the differences are much larger when using the MP2:PM6 scheme, leading to significant variations of the relative β_{HRS} values. Finally, when using the LC-BLYP/6-31+G(d) method to describe the high layer, the β_{HRS} values are systematically smaller than those obtained with MP2:HF, but a better ordering is obtained than at the MP2:PM6 level.

IV. COMPARISON WITH EXPERIMENT AND FURTHER DISCUSSION

Table 6 displays the β_{HRS} extracted from the measurements as well as the corresponding static values extrapolated using the two-state approximation incorporating an inhomogeneous broadening based on parameters fitted to the absorption spectrum.[57] These quantities are compared to a selection of values computed for a wavelength of 1900 nm. This wavelength is necessary for avoiding biased comparisons because the static and dynamic dielectric constants differ much. On the other hand, this wavelength is large enough to prevent (near) resonance effects. As discussed in Section III, quantitative and qualitative deviations are observed when (i) the high layer is treated at the HF level, (ii) the low layer is described using PM6, and (iii) the remaining environment is not modeled by a polarizable continuum. Globally, the MP2/IEFPCM results on the chromophores (and the π-stacked residue on the phenolate, when present) reproduce the experimental trends within the experimental error bars. Still, the β_{HRS} values are overestimated, with larger deviations for eYFP, eGFP, and SHardonnay, which possess a similar chromophore structure. These MP2/IEFPCM values account for the decrease of β_{HRS} by going from SHardonnay to eYFP, in agreement with the appearance of local centrosymmetry due to the π-stacking interactions between the chromophore and TYR 203 in eYFP, whereas in SHardonnay, TYR 203 is replaced by PHE 203. Very similar trends are observed at the MP2:HF/IEF-PCM level, with the exception of the relative values for eYFP and eGFP that are inverted.

Still, at (almost) all levels of approximation, in agreement with experiment, the mCherry HRS response is the largest, followed by ZsYellow and DsRed, which present similar values. Their chromophores share in fact the same π-conjugated segment, where the N=C double bond of the imidazolone is in resonance with an exo imine (ZsYellow) or acylimine (DsRed and mCherry) (Figure 4), whereas there is no such π-conjugation in the three other FPs. This extension of the π-

DOI: 10.1021/acs.jpcb.8b01430
J. Phys. Chem. B 2018, 122, 4993−5005

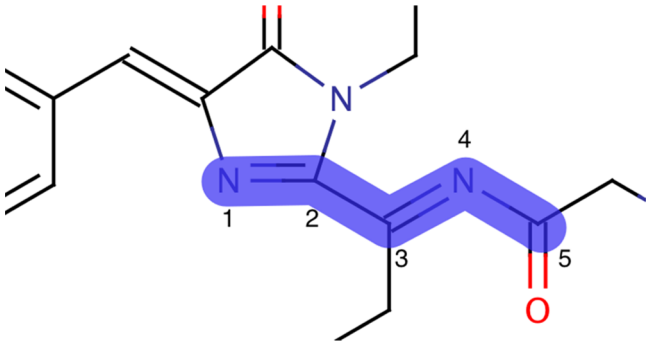

Figure 4. Sketch of the bonds accounted for when calculating the bond length alternation (BLA).

conjugation segment in mCherry, ZsYellow, and DsRed explains their larger β values, in agreement with previous investigations.[42] Still, the π-conjugation is much different from ZsYellow to DsRed and mCherry, as evidenced by the bond length alternation (BLA) along the N(1)═C(2)−C(3)═N(4) π-conjugated segment, as obtained from X-ray diffraction data, which goes from 0.25 to 0.17 and to 0.00 Å, respectively. These BLA differences account partly for the fact that β_{HRS} (mCherry) = 156 × 10^2 au > β_{HRS} (DsRed) = 111 × 10^2 au > β_{HRS} (ZsYellow) = 94 × 10^2 au, as determined at the MP2:HF/IEFPCM level. On the other hand, their crystal structures are similar for the N(1)═C(2)−C(3)═N(4) torsion angles (179.6, 173.2, and 179.1° for ZsYellow, DsRed, and mCherry, respectively), highlighting also a favored conjugation due to planarity. Obviously, the same torsion angle is much different in eGFP (90.0°), eYFP (101.6°), and SHardonnay (100.7°) due to the lack of π-conjugation. Moreover, the C═O bond orientation is almost perpendicular to the π-conjugated segment plane for both mCherry and DsRed, but a change of orientation occurs for a different bond ($\theta_{C(3)=N(4)-C(5)=O}$ = 119.7° for DsRed and $\theta_{C(2)-C(3)=N(4)-C(5)}$ = 102.18° for mCherry).

Table 7 presents the depolarization ratios calculated at the two highest levels of theory considered in this study, i.e., the ONIOM MP2/6-31+G(d):HF/6-31+G(d)/IEFPCM level for the deprotonated chromophores in its protein environment and at the MP2/6-31+G(d)/IEFPCM level for the deprotonated chromophores sketched in Figure 1, considering water as solvent. All DR values are close to 5.0, which is the typical value for one-dimensional chromophore with a dominant/unique β_{iii} diagonal component (where i is along the charge-transfer axis). DR values also demonstrate the dominant dipolar character of the β_{HRS} response and its small enhancement for chromophores with a larger π-conjugated moiety.

Improving these comparisons and the determination of structure−property relationships are hampered by some difficulties, going beyond the truncation of the protein structure and the use of a polarizable continuum to describe the rest of the surrounding. Indeed, in solution, some of the proteins are in equilibrium with oligomeric complexes. Although mCherry[58] is a monomer, eGFP,[59] eYFP,[59] and SHardonnay monomers are in a weak equilibrium with their dimer forms. Moreover, DsRed[44,46] and ZsYellow[47,48] are tetrameric proteins. Thus, in addition to differences in their environments, the HRS response of these oligomeric proteins depends also on the relative orientation of the chromophores in the different moieties.

V. CONCLUSIONS AND OUTLOOK

The performance of quantum chemistry methods to calculate the second-order nonlinear optical (NLO) properties (at the molecular scale, the first hyperpolarizability, β, of fluorescent proteins (FPs)) has been assessed. This paper adopts the ONIOM scheme, which consists in partitioning the system in several layers treated at different levels of approximation, from the most elaborated method for its core (called the high layer) to the most approximate one for the outer surrounding (called the low layer). The goal is to incorporate the effects of the microenvironment of the chromophore as much as possible on the NLO response of the FP chromophore that is embedded in a protective β-barrel protein cage. A selection of six FPs, for which experimental NLO data are available, has been considered: eGFP, eYFP, SHardonnay, ZsYellow, DsRed, and mCherry.

Calculations demonstrate that predicting and interpreting the second-order NLO responses of FPs is a real challenge for quantum chemistry because of the size of the system, which calls for addressing successive refinements of the ONIOM scheme. We observe that a small high layer can already account for the variations of β as a function of the nature of the FP, provided the low layer is treated at an ab initio level. This is required for a proper description of key H-bondings. Then, both electron correlation and solvent effects are needed for semiquantitative reproduction of the experimental values obtained from hyper-Rayleigh scattering (HRS) experiments, β_{HRS}. Indeed, including electron correlation effects at the second-order Møller−Plesset perturbation theory (MP2) level leads to an increase of the β_{HRS} by a factor of 2.0 ± 0.3, except for SHardonnay, where this factor is larger. This led us to define the MP2/6-31+G(d):HF/6-31+G(d)/IEFPCM scheme as an efficient ONIOM approach and the MP2/6-31+G(d):HF/6-31G(d)/IEFPCM as a better compromise between accuracy and computational needs. These ONIOM results and the corresponding experimental data were then interpreted in terms of structural differences between the FPs, the length of

Table 7. Depolarization Ratios Obtained at the ONIOM MP2/6-31+G(d):HF/6-31+G(d)/IEFPCM Level for the Deprotonated Chromophores in Its Protein Environment and at the MP2/6-31+G(d)/IEFPCM Level for the Deprotonated Chromophores Sketched in Figure 1, Considering Water as Solvent

	MP2/6-31+G(d):HF/6-31+G(d)/IEFPCM	MP2/6-31+G(d)/IEFPCM
eGFP	4.62	4.69
eYFP	4.79	4.76
SHardonnay	4.88	4.84
ZsYellow	5.82	5.87
DsRed	5.11	5.61
mCherry	4.75	5.05

DOI: 10.1021/acs.jpcb.8b01430
J. Phys. Chem. B 2018, 122, 4993−5005

the π-conjugated segment, the variation of the bond length alternation, and the presence of π-stacking interactions, demonstrating the importance of all these parameters. Considering the small diversity of the FP chromophores, these results demonstrate the key role of the β-barrel and surrounding residues. Besides keeping the TYR66 or equivalent side chain in place, it imposes additional differences in geometries with considerable effects on their NLO responses. Concomitantly, this shows the high sensitivity of the NLO responses of the FP chromophores to their environment. Further quantitative comparisons between experiments and calculations are however hampered by the truncated size of the systems and also by the fact that, in solution, several FPs are in equilibrium with their oligomers (dimers for eGFP, eYFP, and SHardonnay; tetramers for DsRed and ZsYellow). A direct and ambitious follow-up of this study will therefore be the investigation of that hypothesis by performing calculations on oligomers.

■ ASSOCIATED CONTENT

Supporting Information

The Supporting Information is available free of charge on the ACS Publications website at DOI: 10.1021/acs.jpcb.8b01430.

Additional static and dynamic hyperpolarizability results for the chromophores in its protein environment; reported calculations deals with electron correlation (MP2 versus HF), with frequency dispersion (TDHF versus CPHF), ONIOM partitioning, and solvent effects (PDF)

■ AUTHOR INFORMATION

Corresponding Author

*E-mail: benoit.champagne@unamur.be.

ORCID

Benoît Champagne: 0000-0003-3678-8875

Present Addresses

[#]Marine Biology, University of California, San Diego, 9500 Gilman Drive #0202, CA La Jolla 92093, United States (E.D.M.).

[⊥]Belgium Institute for Space Aeronomy, Avenue Circulaire 3, B-1180 Bruxelles, Belgium (E.B.).

[∥]Mulliken Center for Theoretical Chemistry, Institut für Physikalische und Theoretische Chemie, University of Bonn, Beringstr. 4, 53115 Bonn, Germany (M.deW.).

Notes

The authors declare no competing financial interest.

■ ACKNOWLEDGMENTS

This work was supported by funds from the Francqui Foundation. The calculations were performed on the computing facilities of the Consortium des Équipements de Calcul Intensif (CÉCI, http://www.ceci-hpc.be), and particularly those of the Technological Platform on High-Performance Computing, for which we gratefully acknowledge the financial support of the FNRS-FRFC (Convention Nos. 2.4.617.07.F and 2.5020.11) and the University of Namur.

■ DEDICATION

This paper is dedicated to the memory of Professor Kenji Morokuma, who has pioneered embedding methods and the ONIOM scheme and with whom some of the authors had the honor to discuss preliminary results of this study.

■ REFERENCES

(1) Campagnola, P. J.; Loew, L. M. Second-Harmonic Imaging Microscopy for Visualizing Biomolecular Arrays in Cells, Tissues and Organisms. *Nat. Biotechnol.* **2003**, *21*, 1356−60.

(2) Reeve, J. E.; Anderson, H. L.; Clays, K. Dyes for Biological Second Harmonic Generation Imaging. *Phys. Chem. Chem. Phys.* **2010**, *12*, 13484−98.

(3) Abraham, T.; Hirota, J. A.; Wadsworth, S.; Knight, D. A. Minimally Invasive Multiphoton and Harmonic Generation Imaging of Extracellular Matrix Structures in Lung Airway and Related Diseases. *Pulm. Pharmacol. Ther.* **2011**, *24*, 487−96.

(4) Strachan, C. J.; Windbergs, M.; Offerhaus, H. L. Pharmaceutical Applications of Non-Linear Imaging. *Int. J. Pharm.* **2011**, *417*, 163−72.

(5) Huang, S. H.; Hsiao, C. D.; Lin, D. S.; Chow, C. Y.; Chang, C. J.; Liau, I. Imaging of Zebrafish in Vivo with Second-Harmonic Generation Reveals Shortened Sarcomeres Associated with Myopathy Induced by Statin. *PLoS One* **2011**, *6*, No. e24764.

(6) Doras, C.; Taupier, G.; Barsella, A.; Mager, L.; Boeglin, A.; Bulou, H.; Bousquet, P.; Dorkenoo, K. D. Polarization State Studies in Second Harmonic Generation Signals to Trace Atherosclerosis Lesions. *Opt. Express* **2011**, *19*, 15062−15068.

(7) Chen, W. L.; Hu, P. S.; Ghazaryan, A.; Chen, S. J.; Tsai, T. H.; Dong, C. Y. Quantitative Analysis of Multiphoton Excitation Autofluorescence and Second Harmonic Generation Imaging for Medical Diagnosis. *Comput. Med. Imaging Graphics* **2012**, *36*, 519−526.

(8) Chen, X.; Nadiarynkh, O.; Plotnikov, S.; Campagnola, P. J. Second Harmonic Generation Microscopy for Quantitative Analysis of Collagen Fibrillar Structure. *Nat. Protoc.* **2012**, *7*, 654−69.

(9) Wu, S.-L.; Li, H.; Zhang, X. M.; Chen, W. R.; Wang, Y. X. Character of Skin on Photo-Thermal Response and its Regeneration Process using Second-Harmonic Generation Microscopy. *Lasers Med. Sci.* **2013**, 141−146.

(10) Pavone, F. S.; Campagnola, P. J. *Second Harmonic Generation Imaging*; Taylor & Francis, 2013.

(11) Deniset-Besseau, A.; Duboisset, J.; Benichou, E.; Hache, F.; Brevet, P.-F.; Schanne-Klein, M.-C. Measurement of the Second-Order Hyperpolarizability of the Collagen Triple Helix and Determination of Its Physical Origin. *J. Phys. Chem. B* **2009**, *113*, 13437−13445.

(12) de Wergifosse, M.; de Ruyck, J.; Champagne, B. How the Second-Order Nonlinear Optical Response of the Collagen Triple Helix Appears: A Theoretical Investigation. *J. Phys. Chem. C* **2014**, *118*, 8595−8602.

(13) Harczuk, I.; Vahtras, O.; Ågren, H. First Hyperpolarizability of Collagen Using the Point Dipole Approximation. *J. Phys. Chem. Lett.* **2016**, *7*, 2132−2138.

(14) Campagnola, P. Second Harmonic Generation Imaging Microscopy: Applications to Diseases Diagnostics. *Anal. Chem.* **2011**, *83*, 3224−3231.

(15) Chalfie, M. GFP: Lighting Up Life (Nobel Lecture). *Angew. Chem., Int. Ed.* **2009**, *48*, 5603−5611.

(16) Shimomura, O. Discovery of Green Fluorescent Protein (GFP) (Nobel Lecture). *Angew. Chem., Int. Ed.* **2009**, *48*, 5590−5602.

(17) Tsien, R. Y. Constructing and Exploiting the Fluorescent Protein Paintbox (Nobel Lecture). *Angew. Chem., Int. Ed.* **2009**, *48*, 5612−5626.

(18) Lewis, A.; Khatchatouriants, A.; Treinin, M.; Chen, Z.; Peleg, G.; Friedman, N.; Bouevitch, O.; Rothman, Z.; Loew, L.; Sheres, M. Second-Harmonic Generation of Biological Interfaces: Probing the Membrane Protein Bacteriorhodopsin and Imaging Membrane Potential around GFP Molecules at Specific Sites in Neuronal Cells of C. elegans. *Chem. Phys.* **1999**, *245*, 133−144.

(19) Khatchatouriants, A.; Lewis, A.; Rothman, Z.; Loew, L.; Treinin, M. GFP Is a Selective Non-Linear Optical Sensor of Electrophysiological Processes in Caenorhabditis elegans. *Biophys. J.* **2000**, *79*, 2345−2352.

DOI: 10.1021/acs.jpcb.8b01430
J. Phys. Chem. B 2018, 122, 4993−5005

(20) Asselberghs, I.; Flors, C.; Ferrighi, L.; Botek, E.; Champagne, B.; Mizuno, H.; Ando, R.; Miyawaki, A.; Hofkens, J.; Van der Auweraer, M.; Clays, K. Second-Harmonic Generation in GFP-like Proteins. *J. Am. Chem. Soc.* **2008**, *130*, 15713−15719.
(21) De Meulenaere, E.; Asselberghs, I.; de Wergifosse, M.; Botek, E.; Spaepen, S.; Champagne, B.; Vanderleyden, J.; Clays, K. Second-Order Nonlinear Optical Properties of Fluorescent Proteins for Second-Harmonic Imaging. *J. Mater. Chem.* **2009**, *19*, 7514−7519.
(22) De Meulenaere, E.; de Wergifosse, M.; Botek, E.; Spaepen, S.; Champagne, B.; Vanderleyden, J.; Clays, K. Nonlinear Optical Properties of mStrawberry and mCherry for Second Harmonic Imaging. *J. Nonlinear Opt. Phys. Mater.* **2010**, *19*, 1−13.
(23) De Meulenaere, E.; Nguyen Bich, N.; de Wergifosse, M.; Van Hecke, K.; Van Meervelt, L.; Vanderleyden, J.; Champagne, B.; Clays, K. Improving the Second-Order Nonlinear Optical Response of Fluorescent Proteins: The Symmetry Argument. *J. Am. Chem. Soc.* **2013**, *135*, 4061−4069.
(24) Dapprich, S.; Komáromi, I.; Byun, K. S.; Morokuma, K.; Frisch, M. J. A New ONIOM Implementation in Gaussian98. Part I. The Calculation of Energies, Gradients, Vibrational Frequencies and Electric Field Derivatives. *J. Mol. Struct.: THEOCHEM* **1999**, *461−462*, 1−21.
(25) Clemente, F. R.; Vreven, T.; Frisch, M. J. Getting the Most out of ONIOM: Guidelines and Pitfalls. In *Quantum Biochemistry*; Wiley-VCH Verlag GmbH & Co. KGaA, 2010; pp 61−83.
(26) Vreven, T.; Byun, K. S.; Komáromi, I.; Dapprich, S.; Montgomery, J. A.; Morokuma, K.; Frisch, M. J. Combining Quantum Mechanics Methods with Molecular Mechanics Methods in ONIOM. *J. Chem. Theory Comput.* **2006**, *2*, 815−826.
(27) Chung, L. W.; Sameera, W. M. C.; Ramozzi, R.; Page, A. J.; Hatanaka, M.; Petrova, G. P.; Harris, T. V.; Li, X.; Ke, Z.; Liu, F.; Li, H.-B.; Ding, L.; Morokuma, K. The ONIOM Method and Its Applications. *Chem. Rev.* **2015**, *115*, 5678−5796.
(28) Li, X.; Chung, L. W.; Mizuno, H.; Miyawaki, A.; Morokuma, K. Competitive Mechanistic Pathways for Green-to-Red Photoconversion in the Fluorescent Protein Kaede: a Computational Study. *J. Phys. Chem. B* **2010**, *114*, 16666−16675.
(29) Li, X.; Chung, L. W.; Mizuno, H.; Miyawaki, A.; Morokuma, K. A Theoretical Study on the Nature of On- and Off-States of Reversibly Photoswitching Fluorescent Protein Dronpa: Absorption, Emission, Protonation, and Raman. *J. Phys. Chem. B* **2010**, *114*, 1114−1126.
(30) Matsuura, A.; Hayashi, T.; Sato, H.; Takahashi, A.; Sakurai, M. Theoretical Study on the Absorption Maxima of Real GFPs. *Chem. Phys. Lett.* **2010**, *484*, 324−329.
(31) Ma, Y.; Sun, Q.; Li, Z.; Yu, J. G.; Smith, S. C. Theoretical Studies of Chromophore Maturation in the Wild-Type Green Fluorescent Protein: ONIOM(DFT:MM) Investigation of the Mechanism of Cyclization. *J. Phys. Chem. B* **2012**, *116*, 1426−36.
(32) Bhattacharya, D.; Panda, A.; Shil, S.; Goswami, T.; Misra, A. A Theoretical Study on Photomagnetic Fluorescent Protein Chromophore Coupled Diradicals and their Possible Applications. *Phys. Chem. Chem. Phys.* **2012**, *14*, 6905−6913.
(33) Ding, L.; Chung, L. W.; Morokuma, K. Reaction Mechanism of Photoinduced Decarboxylation of the Photoactivatable Green Fluorescent Protein: An ONIOM(QM:MM) Study. *J. Phys. Chem. B* **2013**, *117*, 1075−1084.
(34) Thompson, L. M.; Lasoroski, A.; Champion, P. M.; Sage, J. T.; Frisch, M. J.; van Thor, J. J.; Bearpark, M. J. Analytical Harmonic Vibrational Frequencies for the Green Fluorescent Protein Computed with ONIOM: Chromophore Mode Character and Its Response to Environment. *J. Chem. Theory Comput.* **2014**, *10*, 751−766.
(35) Steindal, A. H.; Olsen, J. M. H.; Ruud, K.; Frediani, L.; Kongsted, J. A Combined Quantum Mechanics/Molecular Mechanics Study of the One- and Two-Photon Absorption in the Green Fluorescent Protein. *Phys. Chem. Chem. Phys.* **2012**, *14*, 5440−5451.
(36) List, N. H.; Olsen, J. M. H.; Jensen, H. J. A.; Steindal, A. H.; Kongsted, J. Molecular-Level Insight into the Spectral Tuning Mechanism of the DsRed Chromophore. *J. Phys. Chem. Lett.* **2012**, *3*, 3513−3521.
(37) Steindal, A. H.; Beerepoot, M. T. P.; Ringholm, M.; List, N. H.; Ruud, K.; Kongsted, J.; Olsen, J. M. H. Open-Ended Response Theory with Polarizable Embedding: Multiphoton Absorption in Biomolecular Systems. *Phys. Chem. Chem. Phys.* **2016**, *18*, 28339−28352.
(38) Stewart, J. J. Optimization of Parameters for Semi-empirical Methods V: Modification of NDDO Approximations and Application to 70 elements. *J. Mol. Model.* **2007**, *13*, 1173−213.
(39) Champagne, B.; Perpète, E. A.; Jacquemin, D.; van Gisbergen, S. J. A.; Baerends, E.-J.; Soubra-Ghaoui, C.; Robins, K. A.; Kirtman, B. Assessment of Conventional Density Functional Schemes for Computing the Dipole Moment and (Hyper)polarizabilities of Push−Pull π-Conjugated Systems. *J. Phys. Chem. A* **2000**, *104*, 4755−4763.
(40) Suponitsky, K. Y.; Tafur, S.; Masunov, A. E. Applicability of hybrid density functional theory methods to calculation of molecular hyperpolarizability. *J. Chem. Phys.* **2008**, *129*, No. 044109.
(41) Suponitsky, K. Y.; Liao, Y.; Masunov, A. E. Electronic Hyperpolarizabilities for Donor−Acceptor Molecules with Long Conjugated Bridges: Calculations versus Experiment. *J. Phys. Chem. A* **2009**, *113*, 10994−11001.
(42) de Wergifosse, M.; Champagne, B. Electron Correlation Effects on the First Hyperpolarizability of Push-Pull π-Conjugated Systems. *J. Chem. Phys.* **2011**, *134*, No. 074113.
(43) Champagne, B.; Beaujean, P.; de Wergifosse, M.; Cardenuto, M. H.; Liégeois, V.; Castet, F. Quantum Chemical Methods for Predicting and Interpreting Second-Order Nonlinear Optical Properties: From Small to Extended π-Conjugated Molecules. In *Frontiers of Quantum Chemistry*; Wójcik, M. J., Nakatsuji, H., Kirtman, B., Ozaki, Y., Eds.; Springer: Singapore, 2018; pp 117−138.
(44) Elsliger, M.-A.; Wachter, R. M.; Hanson, G. T.; Kallio, K.; Remington, S. J. Structural and Spectral Response of Green Fluorescent Protein Variants to Changes in pH. *Biochemistry* **1999**, *38*, 5296−5301.
(45) Wachter, R. M.; Elsliger, M.-A.; Kallio, K.; Hanson, G. T.; Remington, S. J. Structural Basis of Spectral Shifts in the Yellow-Emission Variants of Green Fluorescent Protein. *Structure* **1998**, *6*, 1267−1277.
(46) Yarbrough, D.; Wachter, R. M.; Kallio, K.; Matz, M. V.; Remington, S. J. Refined Crystal Structure of DsRed, a Red Fluorescent Protein from Coral, at 2.0-Å resolution. *Proc. Natl. Acad. Sci. U.S.A.* **2001**, *98*, 462−467.
(47) Shu, X.; Shaner, N. C.; Yarbrough, C. A.; Tsien, R. Y.; Remington, S. J. Novel Chromophores and Buried Charges Control Color in mFruits. *Biochemistry* **2006**, *45*, 9639−9647.
(48) Remington, S. J.; Wachter, R. M.; Yarbrough, D. K.; Branchaud, B.; Anderson, D. C.; Kallio, K.; Lukyanov, K. A. zFP538, a Yellow-Fluorescent Protein from Zoanthus, Contains a Novel Three-Ring Chromophore. *Biochemistry* **2005**, *44*, 202−212.
(49) Stewart, J. *MOPAC2009, Stewart Computational Chemistry*; Colorado Springs: CO, 2009.
(50) Mohammed, A. A. K.; Limacher, P. A.; Champagne, B. Finding Optimal Finite Field Strengths Allowing for a Maximum of Precision in the Calculation of Polarizabilities and Hyperpolarizabilities. *J. Comput. Chem.* **2013**, *34*, 1497−1507.
(51) de Wergifosse, M.; Liégeois, V.; Champagne, B. Evaluation of the Molecular Static and Dynamic First Hyperpolarizabilities. *Int. J. Quantum Chem.* **2014**, *114*, 900−910.
(52) Patel, A. H. G.; Mohammed, A. A. K.; Limacher, P. A.; Ayers, P. W. Finite Field Method for Nonlinear Optical Property Prediction Using Rational Function Approximants. *J. Phys. Chem. A* **2017**, *121*, 5313−5323.
(53) Tomasi, J.; Mennucci, B.; Cammi, R. Quantum Mechanical Continuum Solvation Models. *Chem. Rev.* **2005**, *105*, 2999−3094.
(54) Tomasi, J.; Persico, M. Molecular Interactions in Solution: An Overview of Methods Based on Continuous Distributions of the Solvent. *Chem. Rev.* **1994**, *94*, 2027−2094.
(55) Vreven, T.; Mennucci, B.; da Silva, C. O.; Morokuma, K.; Tomasi, J. The ONIOM-PCM Method: Combining the Hybrid Molecular Orbital Method and the Polarizable Continuum Model for

DOI: 10.1021/acs.jpcb.8b01430
J. Phys. Chem. B 2018, 122, 4993−5005

Solvation. Application to the Geometry and Properties of a Merocyanine in Solution. *J. Chem. Phys.* **2001**, *115*, 62−72.
(56) Frisch, M. J.; Trucks, G. W.; Schlegel, H. B.; Scuseria, G. E.; Robb, M. A.; Cheeseman, J. R.; Scalmani, G.; Barone, V.; Mennucci, B.; Petersson, G. A. et al. *Gaussian 09*, revision A.01; Gaussian, Inc.: Wallingford CT, 2009.
(57) Campo, J.; Wenseleers, W.; Goovaerts, E.; Szablewski, M.; Cross, G. H. Accurate Determination and Modeling of the Dispersion of the First Hyperpolarizability of an Efficient Zwitterionic Nonlinear Optical Chromophore by Tunable Wavelength Hyper-Rayleigh Scattering. *J. Phys. Chem. C* **2008**, *112*, 287−296.
(58) Shaner, N. C.; Steinbach, P. A.; Tsien, R. Y. A Guide to Choosing Fluorescent Proteins. *Nat. Methods* **2005**, *2*, 905−909.
(59) Shaner, N. C.; Campbell, R. E.; Steinbach, P. A.; Giepmans, B. N. G.; Palmer, A. E.; Tsien, R. Y. Improved Monomeric Red, Orange and Yellow Fluorescent Proteins Derived from Discosoma sp. red Fluorescent Protein. *Nat. Biotechnol.* **2004**, *22*, 1567−1572.

DOI: 10.1021/acs.jpcb.8b01430
J. Phys. Chem. B 2018, 122, 4993−5005